PCCP

ROYAL SOCIETY OF CHEMISTRY

PAPER

View Article Online
View Journal | View Issue

Cite this: *Phys. Chem. Chem. Phys.*, 2020, **22**, 20394

Unimolecular decomposition of methyl ketene and its dimer in the gas phase: theory and experiment†

Imene Derbali,[a] Helgi Rafn Hrodmarsson, *[bc] Martin Schwell,[d] Yves Bénilan,[d] Lionel Poisson,[e] Majdi Hochlaf, *[f] Mohammad Esmaïl Alikhani,[a] Jean-Claude Guillemin[g] and Emilie-Laure Zins[a]

We present a combined theoretical and experimental investigation on the single photoionization and dissociative photoionization of gas-phase methyl ketene (MKE) and its neutral dimer (MKE_2). The performed experiments entail the recording of photoelectron photoion coincidence (PEPICO) spectra and slow photoelectron spectra (SPES) in the energy regime 8.7–15.5 eV using linearly polarized synchrotron radiation. We observe both dimerization and trimerization of the monomer which brings about significantly complex and abstruse dissociative ionization patterns. These require the implementation of theoretical calculations to explore the potential energy surfaces of the monomer and dimer's neutral and ionized geometries. To this end, explicitly correlated quantum chemical methodologies involving the coupled cluster with single, double and perturbative triple excitations (R)CCSD(T)-F12 method, are utilized. An improvement in the adiabatic ionization energy of MKE is presented (AIE = 8.937 ± 0.020 eV) as well as appearance energies for multiple fragments formed through dissociative ionization of either the MKE monomer or dimer. In this regard, the synergy of experiment and theory is crucial to interpreting the obtained results. We discuss the potential astrochemical implications of this work in the context of recent advances in the field of astrochemistry and speculate on the potential presence and eventual fate of interstellar MKE molecules.

Received 23rd July 2020,
Accepted 26th August 2020

DOI: 10.1039/d0cp03921g

rsc.li/pccp

1. Introduction

A key question in astrophysics, astrochemistry, and astrobiology concerns the origins of molecular complexity in space.[1–3] At the time of writing, well over 200 molecules have been detected in the interstellar medium (ISM); approximately one third of them being complex organics molecules (COMs) containing six atoms or more.[4] COMs have been shown to effectively form upon VUV photoprocessing of simple interstellar ice analogs[5–8] but to explain their abundance in the gas phase in cold molecular clouds requires a VUV- (or cosmic ray) driven photodesorption paradigm to complement thermal desorption.[1] Ultracold gas phase reaction kinetics measurements have, however, shown that chemical kinetics display significantly anti-Arrhenius kinetics at temperatures approaching that of the interstellar medium (ISM).[9,10] The recent detection of cyanobenzene in the TMC-1 molecular cloud,[11] and the assignment of several of the diffuse interstellar bands (DIBs) to transitions within the C_{60}^+ Buckyball cation,[12] have now challenged our basic notions of molecular complexity in space and the upper limits to interstellar molecular complexity are quickly extending.

A significant portion of the COMs that have been detected in space are linear rigid carbon chains. These may include nitrogen (such as cyanopolyynes[13]) and oxygen (such as the HC_7O radical[14] and ketene; $H_2C{=}C{=}O$[15]). A clear understanding of the VUV photodynamics (including that of photoionization and photofragmentation) of these species and their derivatives is crucial for further interpretation of astronomical data and the modelling of the chemistry of interstellar media.

Methyl ketene ($H_3C{-}CH{=}C{=}O$; 1-propen-1-one), called MKE in the following, is a carbon chain molecule comprising

[a] *MONARIS UMR 8233 CNRS, Sorbonne Université, 4 Place Jussieu, 75252 Paris Cedex 5, France*
[b] *Synchrotron SOLEIL, L'Orme des Merisiers, St Aubin, BP 48, Gif sur Yvette, France*
[c] *Laboratory for Astrophysics, Leiden Observatory, Leiden University, PO Box 9513, NL-2300 RA Leiden, The Netherlands. E-mail: hr.hrodmarsson@gmail.com, hrodmarsson@strw.leidenuniv.nl; Tel: +31 629 413 569*
[d] *LISA UMR 7583 Université Paris-Est Créteil and Université de Paris, Institut Pierre et Simon Laplace, 61 Avenue du Général de Gaulle, 94010 Créteil, France*
[e] *Université Paris-Saclay, CEA, CNRS, LIDYL, 91191 Gif-sur-Yvette, France*
[f] *Université Gustave Eiffel, COSYS/LISIS, 5 Bd Descartes 77454, Champs sur Marne, France. E-mail: hochlaf@univ-mlv.fr*
[g] *Univ Rennes, École Nationale Supérieure de Chimie de Rennes, CNRS, ISCR-UMR6226, F-35000 Rennes, France*

† Electronic supplementary information (ESI) available. See DOI: 10.1039/d0cp03921g

a rigid CCO frame which is of astronomical interest, and whose VUV laboratory data is scarce.[16] Other prior work pertaining to MKE include *e.g.* potential energy surface calculations[17] and characterization of its infrared bands.[18] Recently, Bermúdez *et al.*[19] recorded its mm-wave spectrum in the 50–330 GHz range, and those spectra were used to search for MKE in various interstellar molecular inventories such as Sagittarius B2 and TMC-1 in the Taurus Molecular Cloud, but unsuccessfully. Astronomically, MKE is still expected to play a role as its isomer, propenal ($H_2C{=}CH{-}CHO$), which is merely 2.8 kJ mol^{-1} more stable than MKE according to theory,[19] has been tentatively detected in Sagittarius B2.[20] In order to further contextualize this current non-detection of MKE, particularly in the light of its homolog ketene ($H_2C{=}C{=}O$) having been detected in the 1970's,[15] its VUV photodynamics are of great relevance.

Further indications of the astronomical relevance of MKE have been found in laboratory ice chemistry. MKE has been formed in certain interstellar ice analogues which were inspected in order to find a potential link to the formation of propylene oxide, the first chiral molecule to be detected in the ISM.[20] A potential paradigm of MKE's chemical evolution could involve formation on icy grains and subsequently undergo further chemical reactions, and/or thermal, chemical, or photo-induced desorption. The recent detection of propylene oxide makes a strong case for the detection of MKE as both species can form in such icy grains. A problem with the determination of MKE formation in ices is that the ν_4 fundamental band of MKE overlaps with the infrared stretching vibration of CO. Hence, threshold photoelectron spectroscopy has been suggested as a desirable method to determine the formation of MKE in ices.[21] A similar methodology has been applied to infer the formation of MKE in the reaction between the methylidene radical and acetaldehyde using a multiplexed photoionization mass spectrometer[22] but using a previously recorded photoelectron spectrum of MKE[16] to identify it as a product in the reaction.

Here we present a combined experimental and theoretical study of the photoionization and photofragmentation dynamics of MKE and its dimer, including their threshold photoionization spectra. This continues ongoing work of dedicated and synergistic experimental and theoretical characterizations of astrochemically/astrobiologically relevant molecules.[23–29] Our results are discussed in context of modern advances in experimental astrochemistry and the potential presence of gaseous MKE in space.

2. Methods

2.1 Experimental

Experiments were performed at the DESIRS VUV beamline at the SOLEIL synchrotron in Saint-Aubin, France.[30] Horizontally polarized radiation in the 8.7–15.5 eV range was generated by an undulator[31] and passed through a gas filter filled with Argon to suppress higher harmonics from the undulator by four to five orders of magnitude. The photon beam was dispersed by a 6.65 m normal incidence monochromator with 200 grooves per mm grating. The photon flux of the resulting beam was between 10^{12} and 10^{13} photons per second and was directed into the beamline endstation where the SAPHIRS chamber is located.[32] It contains the DELICIOUS III double-imaging photoion photoelectron coincidence (i^{2}PEPICO) spectrometer[33] in which the synchrotron radiation was interfaced with a molecular beam under a right angle. The generated photoelectrons and photoions are accelerated in opposite directions with a DC electric field of 1000 V. The electron side contains a velocity map imaging spectrometer and the ion side a modified Wiley McLaren time-of-flight 3D momentum imaging spectrometer. This setup allows a PEPICO scheme to be employed, mass-tagging the recorded electron images and eliminating any spurious background compounds.

MKE was produced by pyrolysis at 600 °C under 0.1 mbar of the commercially available propionic anhydride. The by-product propanoic acid was removed by selective condensation in a first U-tube immersed in a cold bath at −70 °C while the formed MKE was trapped in a second U-tube immersed in a 77 K bath. This trap was then fitted on the spectrometer and allowed to warm to −120 °C by immersion in a cooled isopentane bath.

It is thus easily vaporized into a He gas stream that flows through the first gas nozzle inside the differentially pumped SAPHIRS jet chamber, using a backing pressure of approximately 500 mbar. This gas flow is then streamed through a second 50 μm pinhole nozzle leading to the ionization chamber. The applied electric field in the ionization source of DELICIOUS III induces a Stark effect which effectively decreases the ionization energies of the compounds entering the chamber. The Stark effect is approximately 23.5 meV and is corrected for in the energy calibration which uses the signals of ionized background O_2. Intensity calibrations were performed using the recorded flux over the appropriate energy range which has been measured with an AXUV100, IRD Si photodiode. Image inversions are performed with the pBASEX algorithm.[34]

To obtain the threshold photoelectron spectrum we employed the slow photoelectron spectroscopic method (SPES) which has been detailed previously.[35] In brief, following the inversion of mass-tagged images recorded with DELICIOUS III, the ionization intensities can be plotted in matrix form as a function of the electron kinetic energy (eKE) and the photon energy. This two-dimension photoelectron spectral matrix (2D-PES matrix) contains a wealth of spectroscopic information and by investigating different "cuts" through the matrix, properties such as photon-dependent electron kinetic energy distributions, partial photoionization cross sections, *etc.* can be obtained.[36] The recorded 2D-PES matrix of MKE (m/z 56) is presented in Fig. S1 in the ESI.†

To extract the SPES from the 2D-PES matrix, the pixel intensities are diagonally integrated along the electron signals from eKE = 0 up to an arbitrary value, eKE_{max}, carefully chosen to find a compromise between signal intensity and energy resolution. The total energy resolution is a convolution of the photon resolution and the electron bandwidth. Typical energy resolutions are approximately 20 meV for eKE_{max} ranging between 50 and 100 meV.[37]

2.2 Theoretical

We performed the geometry optimizations (opt), in the C_1 point group, of neutral and cationic MKE and of its neutral and

ionized dimer using the PBE0 density functional,[38] where the atoms are described by the augmented correlation-consistent aug-cc-pVTZ (aVTZ) basis sets of Dunning and co-workers.[39,40] Subsequently, we computed the harmonic frequencies to assess the minimal nature of the optimized stationary point (all positive frequencies) and on top of that, we deduced their anharmonic frequencies using the second-order vibrational perturbation theory (VPT2) approach.[41,42] These electronic structure computations were done using GAUSSIAN 09 Revision E.[43] The standard options as implemented in this suite of programs were adopted. The GAUSSIAN package was also used to generate the photoelectron spectrum of MKE *via* the derivation of the Franck Condon (FC) factors for the MKE (X) → MKE^+ (X) ionization transition.[44,45] Indeed, the FC analysis was done by means of the time-independent adiabatic Hessian Franck–Condon (TI-AH|FC) model.[46–49] The stick simulated vibrationally resolved electronic spectrum was later convolved with a 20 meV bandwidth Gaussian profile, corresponding to the present experimental resolution.

These density functional theory results were used as starting points for full re-optimization of the neutral and cationic MKE and of the cationic fragments using the explicitly correlated coupled cluster with single, double and perturbative triple excitations (R)CCSD(T)-F12 method,[50–54] and implemented in the MOLPRO package.[55] The atoms were described by the augmented correlation-consistent cc-pVTZ-F12 basis set.[56] Then, single point (SP) computations were done for the inclusion of core-valence (CV),[57] and scalar relativistic[58] effects at the (R)CCSD(T)/cc-pwCVTZ[59] and (R)CCSD(T)/cc-pVTZ-DK,[58,60,61] respectively, using the composite scheme detailed in our previous works.[27] The accuracy of this composite theoretical approach was estimated to be ±10–20 meV.[25] For the MKE dimer, the CV and SR corrections are done on top of the PBE0/aVTZ computations. Although less accurate than the (R)CCSD(T)-F12 based composite scheme computations, the PBE0/aVTZ//+CV+SR methodology is accurate enough for the interpretation of the experimental features measured here.[62] Furthermore, it was checked that the wB97XD functional leads to similar results from a geometrical and energetical point of view. Tables S1 and S2 (ESI†) allow comparison between the geometry and energetics obtained using these two functionals in combination with the aug-cc-pVTZ basis set. For the derivation of the adiabatic ionization energies (AIE) and appearance energies (AE), we refer to our recent results pertaining to propynal.[27] It is worth mentioning that a barrier could be associated to some of the considered fragmentations channels. However, the agreement between the experimental appearance energies and the calculated ones without considering any barrier suggest that all the considered mechanisms are barrierless, concerted mechanisms.

3. Results & discussion

Here, we present the combined experimental and theoretical results pertaining to the single photon ionization of MKE and its dimer in the gas-phase from the ionization threshold to 15.5 eV. It is well documented that organic molecules can easily form clusters in supersonic expansions,[63] and this is indeed the case here for MKE. As will be shown, the experiment and theory complement one another well to shed light on the complications associated with the effects of dissociative ionization following the clustering of MKE monomers.

3.1 Time-of-flight mass spectra (TOF-MS)

Time-of-flight mass spectra (TOF-MS) recorded at photon energies of 12.5 and 15.5 eV are presented in Fig. 1. At 12.5 eV the monomer, the dimer, and the trimer are clearly visible in descending order of intensity at *m*/*z* 56, *m*/*z* 112, and *m*/*z* 168, respectively (Fig. 1a). Larger clusters are not observed. A signal at *m*/*z* 70 is visible as well, corresponding to residual signals of 2-aminoproprionitrile that were used in a prior experiment and whose results are subject to another publication. A weaker residual signal at *m*/*z* 76 is observed as well but the identity of its carrier is unclear. It is possible that it is an impurity from the thermal degradation of propionic anhydride, with the elemental formula $C_3O_2H_8$ (in which case it could be an isomer of propanediol) or $C_2O_3H_2$ (in which case it could be 1,2,4-trioxolane or hydroxyacetic acid).

At 15.5 eV, the dimer and trimer signals are not visible but several masses lighter than the monomer appear in the TOF-MS (Fig. 1b). Here, the parent ion is still the most intense mass peak. The lighter masses include *m*/*z* 55 and 54 with low

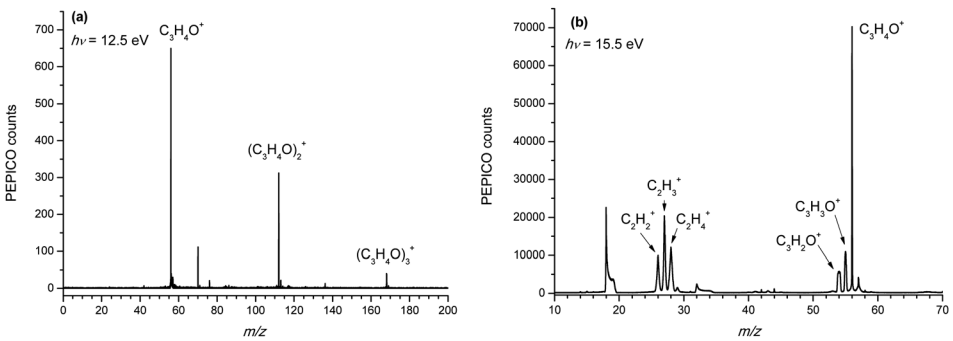

Fig. 1 Time-of-flight mass spectrum (TOF-MS): (a) of MKE, its dimer, and its trimer, photoionized at $h\nu$ = 12.5 eV and (b) of MKE and the different fragments formed by photoionization at $h\nu$ = 15.5 eV.

intensity and correspond to the fragment ions resulting from the loss of atomic and molecular hydrogen to yield $C_3H_3O^+$ and $C_3H_2O^+$, respectively. Other notable fragment signals include $C_2H_4^+$ (m/z 28), $C_2H_3^+$ (m/z 27), and $C_2H_2^+$ (m/z 26). The m/z 57 mass peak corresponds to a mixture of the monomer's ^{13}C isotopomer and the protonated monomer (to be discussed below). Finally, background signals are observed due to ionized residual water (m/z 18) and molecular oxygen (m/z 32) in the ionization chamber. We note that autoionization bands of O_2 were used to calibrate the energy scale of the scan used to record the SPES between 7.8 and 12.5 eV.

3.2 SPES of the MKE monomer

3.2.1 Ground state. Fig. 2 presents the slow photoelectron spectrum (SPES) of the parent ion (m/z 56). The SPES includes a vibrational progression corresponding to the population of the ground electronic state of MKE. The full assignment of the ground state vibrational progression is discussed here below.

The adiabatic ionization energy (AIE) of MKE can be measured from the SPES as the center of the first and most intense band. Here, we deduce a value of $AIE_{exp} = 8.937 \pm 0.020$ eV. To verify this value, we also performed a theoretical calculation of AIE at the (R)CCSD(T)-F12/cc-pVTZ-F12(opt) (+CV + SR + ZPVE) (SP) level and obtained a value of $AIE_{calc} = 8.917$ eV, in good agreement with the experiment. Further details of the calculation, notably geometries of involved neutrals and cations, are presented in Tables S3–S5 of the ESI.† The calculated AIE of MKE is also in agreement with prior VUV photoionization experiments by Bock *et al.* who found a value of 8.95 eV for the adiabatic ionization energy (no precision is given in this earlier work).[16] In this regard, our measurements present an improvement in accuracy.

In their electronic ground states, both neutral MKE and its cation (Fig. 3) belong to the C_s symmetry point group. For neutral MKE, our computed geometry is close to the one calculated earlier by Bak *et al.*[64] Closer inspection of the ionic and neutral equilibrium geometries reveals a subtle geometrical

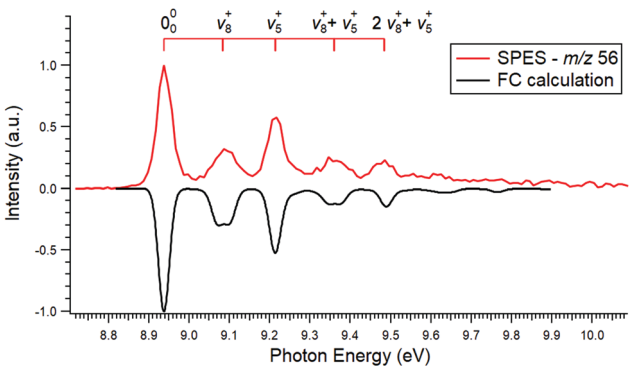

Fig. 2 Experimental (red) and theoretical (black) SPES of the MKE parent ion (m/z 56). The SPES is obtained by using eKE_{max} = 100 meV when diagonally projecting the 2D-PES matrix. The experimental adiabatic ionization energy (AIE) is taken as the median of the 0_0^0 band which is located at 8.937 eV. The assignment of the vibrational progression is discussed in the text. The calculated curve has been shifted upwards in energy by 20 meV to coincide with the experimental results.

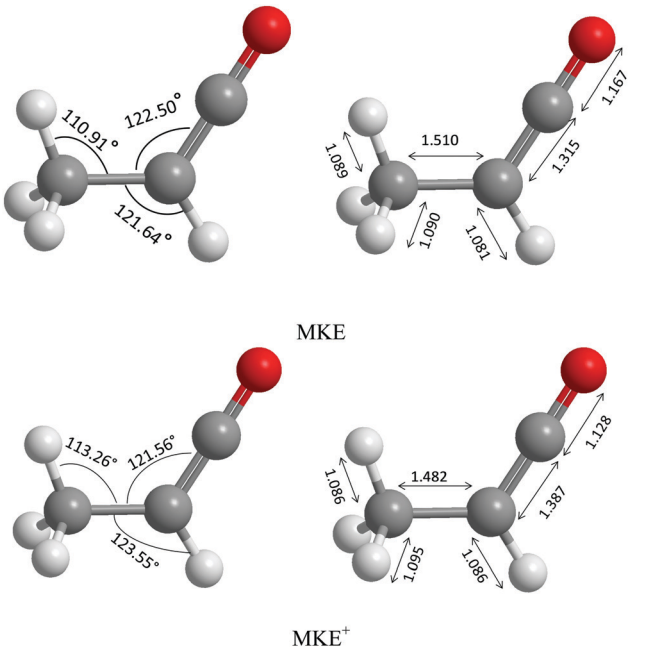

Fig. 3 Main geometrical parameters of the ground of neutral MKE and its cation. Distances are given in Å (right panels) and angles are given in degrees (left panels). These geometries are computed at the (R)CCSD(T)-F12/cc-pVTZ-F12 level.

deformation upon ionization, where the C═O double bond and the C–C single bond slightly contract while the C═C double bond extends. Furthermore, the HCC bond angle of the methyl group changes from 110.91° to 113.26°. These small changes are at the origin of the short vibrational progression in the ground state of MKE^+. Therefore, the general appearance of the SPES spectrum of Fig. 2 can be attributed to the similarities of the equilibrium geometries of the neutral and cationic forms of MKE. Indeed, a short vibrational progression is expected upon ionization of the monomer, in accordance with the FC principle. The recorded SPES typifies this expectation.

The assignment of the monomer's SPES is made possible with quantum chemical calculations. It is guided by the anharmonic wavenumbers calculated for the MKE^+ ground state at the PBE0/aug-cc-pVTZ level of theory. Table 1 presents the anharmonic wavenumbers of the eighteen normal modes of vibration arranged in descending order under a′ and a″ symmetry species. The energies of the observed band maxima in our experiment and comparison with theory are presented in Table 2. Experimental transition energies are also marked by vertical bars in Fig. 2. Below 10 eV these bands are assigned to the photoionization transitions populating the MKE^+ ground state vibrational levels.

The first and most intense band is assigned to the transition of neutral ground state MKE to the ground state of the MKE^+ cation. For the lower intensity band at 9.083 eV ($\nu_{exp}^+ = 1177.6$ cm^{-1}) we propose that it corresponds to the C–C stretching mode between the methyl C-atom and the terminal ketene C-atom. This value is in excellent agreement with the computed value ($\nu_8^+ = 1159.3$ cm^{-1}).

Table 1 Anharmonic wavenumbers (E_{anharm}, cm^{-1} and eV) of the fundamental bands of the ground state of MKE^+ as computed at the PBE0/aug-cc-pVDZ level of theory. We also give their assignment

Vibrational mode	Sym.	E_{anharm} cm^{-1}	E_{anharm} eV	Assignment
ν_1^+	a′	3181.4	0.394	CH (sp^3) stretching
ν_2^+	a′	3155.9	0.391	CH (sp^2) stretching
ν_3^+	a′	3039.3	0.377	CH (sp^3) stretching
ν_4^+	a′	2996.6	0.372	CH_3 sym. stretching
ν_5^+	a′	2298.1	0.285	C═O stretching
ν_6^+	a′	1470.7	0.182	CH (sp^3) in-plane-bending
ν_7^+	a′	1376.3	0.171	C–C stretching
ν_8^+	a′	1159.3	0.144	C–C stretching
ν_9^+	a′	1097.6	0.136	CH_3 (sp^3) asym. stretching
ν_{10}^+	a′	856.1	0.106	CH (sp^3) bending
ν_{11}^+	a′	621.6	0.077	C–C═C in-plane-bending
ν_{12}^+	a′	206.7	0.026	C═C═O in-plane-bending
ν_{13}^+	a′	1408.9	0.175	CH (sp^3) rocking
ν_{14}^+	a′	1309.8	0.162	CH (sp^2) in-plane-bending
ν_{15}^+	a′	931.9	0.116	CH_3 wagging
ν_{16}^+	a′	667.8	0.083	CH (sp^2) out-of-plane-bending
ν_{17}^+	a′	451.4	0.056	C═C═O out-of-plane-bending
ν_{18}^+	a′	119.3	0.015	CH_3 torsion

Table 2 Tentative assignment of the observed vibrational progression resolved in the SPES of the monomer in the 8.7–9.5 eV photon energy range (Fig. 2)

Band position [eV]	Experiment [cm^{-1}]	Theory [cm^{-1}]	Assignment
8.937	0.0[a]	0.0[a]	Adiabatic IE, 0_0^0
9.083	1177.6	1159.3	ν_8^+
9.214	2234.1	2298.1	ν_5^+
9.360	3411.7	3457.4	$\nu_8^+ + \nu_5^+$
9.484	4411.8	4616.7/4596.2/4555.0	$2\nu_8^+ + \nu_5^+/2\nu_5^+$/ $\nu_9^+ + \nu_8^+ + \nu_5^+$

[a] Used as reference.

We propose that the next band in the SPES (ν_{exp}^+ = 2234.1 cm^{-1}) corresponds to the ν_5^+ stretching mode of C═O. The other bands in the SPES can then be tentatively assigned to combination modes of these two ($\nu_8^+ + \nu_5^+$) stretching modes. Comparison between experiment and theory is quite satisfactory (differences are within 50 cm^{-1}) except for the last band observed at 9.484 eV where it exceeds 200 cm^{-1} (or 25 meV). Therefore, we cannot exclude the possibility of either an overtone of the ν_5^+ stretching mode or a contribution from the ν_9 band (corresponding to the asymmetric C–H stretching vibration in the methyl group), resulting in the assignment, *i.e.* $\nu_9^+ + \nu_8^+ + \nu_5^+$.

3.2.2 Dissociative ionization of MKE. Fig. 4 presents the SPES associated with the formation of two cations, namely $C_3H_3O^+$ (m/z 55) and $C_2H_4^+$(m/z 28) which start to appear at around 10 eV. The two fragment ions are also visible in the 15.5 eV TOF-MS presented in Fig. 1b. Both signals are fairly weak and diffuse. Nevertheless, they allow us to measure dissociative ionization thresholds of MKE forming these ionic fragments, which are indicated in Fig. 4.

The m/z 55 SPES corresponds to the loss of an H-atom. From the theoretical calculations on ionization and fragmentation thresholds (see Table 3), it can be inferred that the H loss is

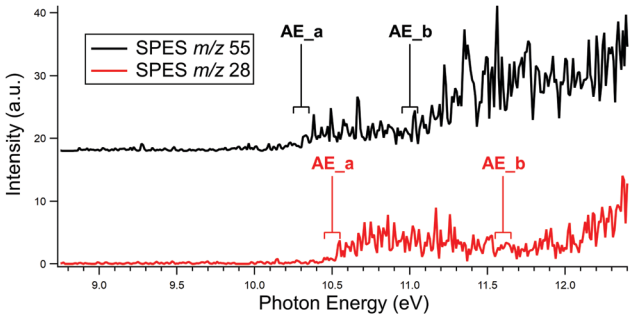

Fig. 4 SPES of two fragments formed by dissociative photoionization of MKE. The m/z 55 fragment ion is shown in black and corresponds to H-loss from the parent cation. The m/z 28 fragment ion is shown in red and corresponds to CO loss from the parent cation. In both the m/z 55 and m/z 28 SPES we observed respectively two appearance energies, AE_a and AE_b, for two fragments, a and b, having the same mass. The ranges of the four AEs are indicated as estimated by the experimental accuracy. See text for further details.

from the methyl group since the experimental onset at AE_b = 11.00 ± 0.05 eV corresponds fairly well to the calculated value of AE_{calc} = 10.78 eV. In the SPES of m/z 55 there seems to be some weak structure between 10.2 eV and 11.0 eV, with an onset energy of approximately 10.2 eV (AE_a). As will be discussed below, this structure may arise from the dissociation of the ionized MKE dimer.

The m/z 28 SPES corresponds to the loss of neutral CO, as is inferred from the quantum chemical calculations (*cf.* Table 3). It shows two bands with origins at AE_a = 10.50 ± 0.05 eV and AE_b = 11.70 ± 0.10 eV (see Fig. 4). In this context, there are two isomers of $C_2H_4^+$ ions that can potentially be formed. The optimized structures of these two considered $C_2H_4^+$ ions are shown in Fig. 5. The two experimental values of the fragment AEs we deduced from the SPES, AE_a and AE_b, are in excellent agreement with the theoretically calculated appearance energies of the two isomers shown in Fig. 5 (AE_{calc1} = 10.508 eV and AE_{calc2} = 11.585 eV; *cf.* Table 3). We can therefore assign the observed m/z 28 thresholds to the formation of two different isomers of $C_2H_4^+$ by dissociative photoionization of MKE.

In order to cover the entire dissociative photoionization potential energy surface of MKE^+, several other fragmentation pathways were considered in the quantum-chemical calculations. They are presented in Fig. 6. The respective calculated AEs are summarized in Table 3 together with some of the results of the calculations and the experimental AEs determined in this work.

Other weaker dissociation channels that may be relevant include the loss of molecular hydrogen, H_2, to form the m/z 54 propadienone isomer ($H_2C{=}C{=}C{=}O^+$). While the m/z 54, 27, and 26 mass signals are too weak to obtain a viable SPES, we can attain an experimental value of the appearance energy by using the point where the ion signals exceed the background signals in their total ion yield curves obtained by accumulating signal at 15.5 eV (Fig. S2 in the ESI†). This method is less accurate than using the SPES but is nonetheless an acceptable form of obtaining approximate fragment appearance energies.[25]

Table 3 Calculated and measured adiabatic ionization energies (AIEs) of MKE and the appearance energies (AEs) of the different fragmentation pathways of the resulting cation (in eV). The most stable structures which correspond to our experimental results are presented. Details of the computational results are given in Table S6 in the ESI

	Ionization	Fragments										
Formula	$C_3H_4O^+$	$C_3H_3O^+$	$C_3H_2O^+$	C_2HO^+	CH_2O^+	HCO^+	$C_2H_4^+$	$C_2H_4^+$_1	CO^+	$C_2H_3^+$	$C_2H_2^+$	CH_3^+
Molecular structures		+H	H_2	CH_3	C_2H_2	C_2H_3	+CO	+CO	C_2H_4	H + CO	H_2 + CO	C_2HO
m/z	56	55	54	41	30	29	28	28	28	27	26	15
AIE or AE calc.	8.917	10.780	12.702	14.756	12.763	12.261	10.508	11.585	14.034	13.205	13.154	13.790
AIE or AE exptl	8.937 ± 0.020	11.00 ± 0.05	12.3 ± 0.1				10.50 ± 0.05	11.60 ± 0.05		13.1 ± 0.1	12.9 ± 0.1	

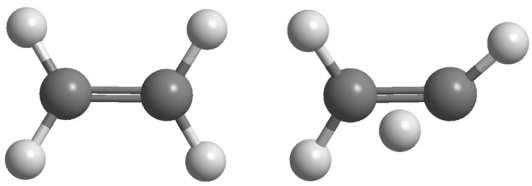

Fig. 5 Optimized structures of two isomers of $C_2H_4^+$ calculated at the (R)CCSD(T)-F12/cc-pVTZ-F12 level. Theoretical AEs are indicated. See text for more details.

For the *m/z* 54 signal, there is a discrepancy between theory and experiment which lies in the AE values. Indeed, the experimental AE value of this fragment from the monomer is 0.4 eV lower than the theoretically derived one. Since the accuracy of the theoretical methodologies is better than 0.4 eV as established in our previous works, the question is raised whether the fragment originates from the monomer at all or whether it originates from dissociative photoionization of the MKE dimer or higher multimers. This is further detailed below.

For the *m/z* 27 and *m/z* 26 fragments, the agreement between experiment and theory is worth mentioning though these discrepancies are somewhat smaller than that for the *m/z* 54 signal (0.1 eV and 0.25 eV, respectively). This could suggest a second mechanism in play in which these fragments are formed by dissociative ionization of the dimer or higher multimers. As with the *m/z* 54 signal, this is discussed below.

3.3 Slow photoelectron spectrum (SPES) of the MKE dimer

3.3.1 Ground state. At higher *m/z* values in the 12.5 eV TOF-MS presented in Fig. 1a, the MKE dimer and trimer (abbreviated MKE_2 and MKE_3) are observed. Here we present the recorded SPES of MKE_2 and discuss its dissociative ionization which affects the monomer signals at energies above the ground state as mentioned above.

To further understand the formation and structure of MKE_2, its structure was theoretically optimized at the PBE0/aVTZ level of theory (see Table S4 of the ESI†). Appearance energies of the fragments $(C_3H_4O)\cdot H^+$ (*m/z* 57) and $(C_3H_5O)\cdot H^+$ (*m/z* 58) are obtained indicating intramolecular H transfer. Indeed, the ionization process of the dimer is accompanied by such intramolecular isomerization and subsequent unimolecular fragmentation processes, as already demonstrated for other organic dimers.[65–67]

Fig. 7 displays the SPES corresponding to the photoionization of MKE_2 (*m/z* 112). The ionization processes remain mainly direct since the energy of the electron distribution rises correspondingly to the photon energy. The SPES comprises a single broad band extending from 8.75 to 9.60 eV where its intensity abruptly drops. The shape of the SPES curve reveals that the photoionization of the dimer results in a broad distribution due to unfavorable FC factors during the $(C_3H_4O)_2 + h\nu \rightarrow (C_3H_4O)_2^+ + e^-$ photoionization transition. This strongly suggests that the structure of the dimer is non-covalent in nature. We also note here that possible covalent dimers (for example 4-ethylidene-3-methyl-2-oxetanone) or other multimers, eventually present in the sample, would certainly possess a saturation vapor pressure that is too low at room temperature in order to be vaporized in our experimental conditions.

To gain a complete understanding of the dimer's VUV photostability, its dissociative ionization requires the implementation of theoretical calculations. The optimized equilibrium molecular structures of the neutral dimer, MKE_2, and its cation, MKE_2^+, are shown in Fig. 8 as computed at the PBE0/aug-cc-pVTZ level. All bond distances are summarized in Table 4. As can be seen, the structure of MKE_2 undergoes a significant geometry change upon ionization. These changes are at the origin of the unfavorable FC factors causing the shape of the broad unstructured band in the dimer's SPES. This is perfectly consistent with our expectations from the FC principle.[45]

3.3.2 Dissociative photoionization of MKE_2 – formation of *m/z* 58, 57, 55, 54, 27, 26. The abrupt decrease in the SPES signal of the dimer combined with the optimized geometries of its neutral and cationic forms are an indication of a dissociative ionization process. To gain a clearer understanding of the potential products formed through dissociative ionization of the MKE dimer, various fragmentation channels, presented as a scheme in Fig. 9, were quantum-chemically investigated.

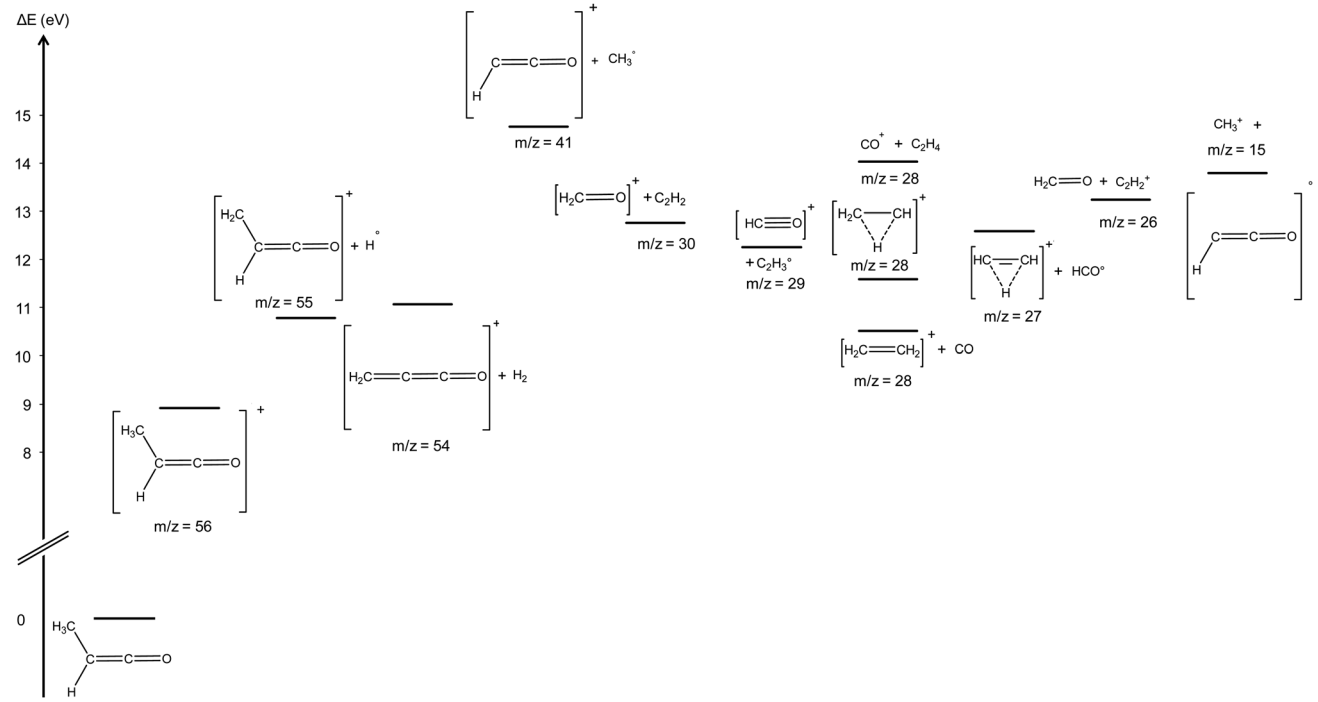

Fig. 6 Dissociative ionziation fragmentation pathways of the MKE cation considered in the quantum-chemical calculations and relative energies (ordinate) compared to the neutral MKE. The abscissa corresponds to descending *m*/*z* values of the formed cationic fragments.

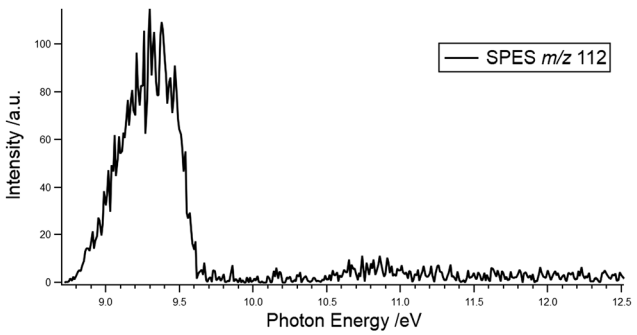

Fig. 7 The SPES corresponding to MKE_2 (*m*/*z* 112).

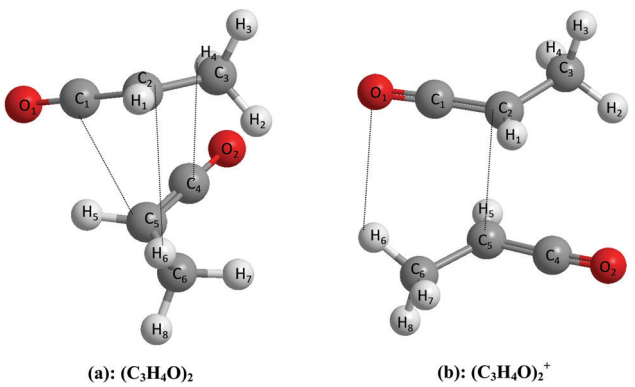

Fig. 8 Optimized geometries of MKE_2 (a) and its cation (b).

Our theoretical and experimental results are presented in Table 5 where values of the respective AEs together with the AIE of MKE_2 are tabulated. Further computational details are given in Table S7 of the ESI.†

There is a large discrepancy between the measured and the calculated AIE of MKE_2 (about 0.9 eV), where the theoretical value is lower than the experimental one by ~0.9 eV. This comes from the large changes, at least, on the intermonomer distances which shrink upon ionization. Consequently, we expect unfavorable FC factors for population of the low vibrational

Table 4 Bond distances defining the equilibrium molecular structure of MKE_2 and of its cation in their electronic ground states. These parameters are computed at the PBE0/aug-cc-pVTZ level of theory. Distances are presented in Å. See Fig. 8 for the numbering of the atoms

	$(C_3H_4O)_2$	$(C_3H_4O)_2^+$
O_1–C_1	1.162	1.140
C_1–C_2	1.307	1.342
C_2–C_3	1.502	1.497
C_2–H_1	1.084	1.087
C_3–H_2	1.093	1.091
C_3–H_3	1.092	1.094
C_3–H_4	1.089	1.088
O_2–C_4	1.162	1.140
C_4–C_5	1.306	1.342
C_5–C_6	1.502	1.496
C_6–H_5	1.083	1.086
C_6–H_6	1.093	1.092
C_6–H_7	1.090	1.088
C_6–H_8	1.092	1.094
C_2–C_5		2.746
O_1–H_6		2.716
C_4–H_4	2.926	
C_2–H_6	3.036	
C_1–C_5	3.383	

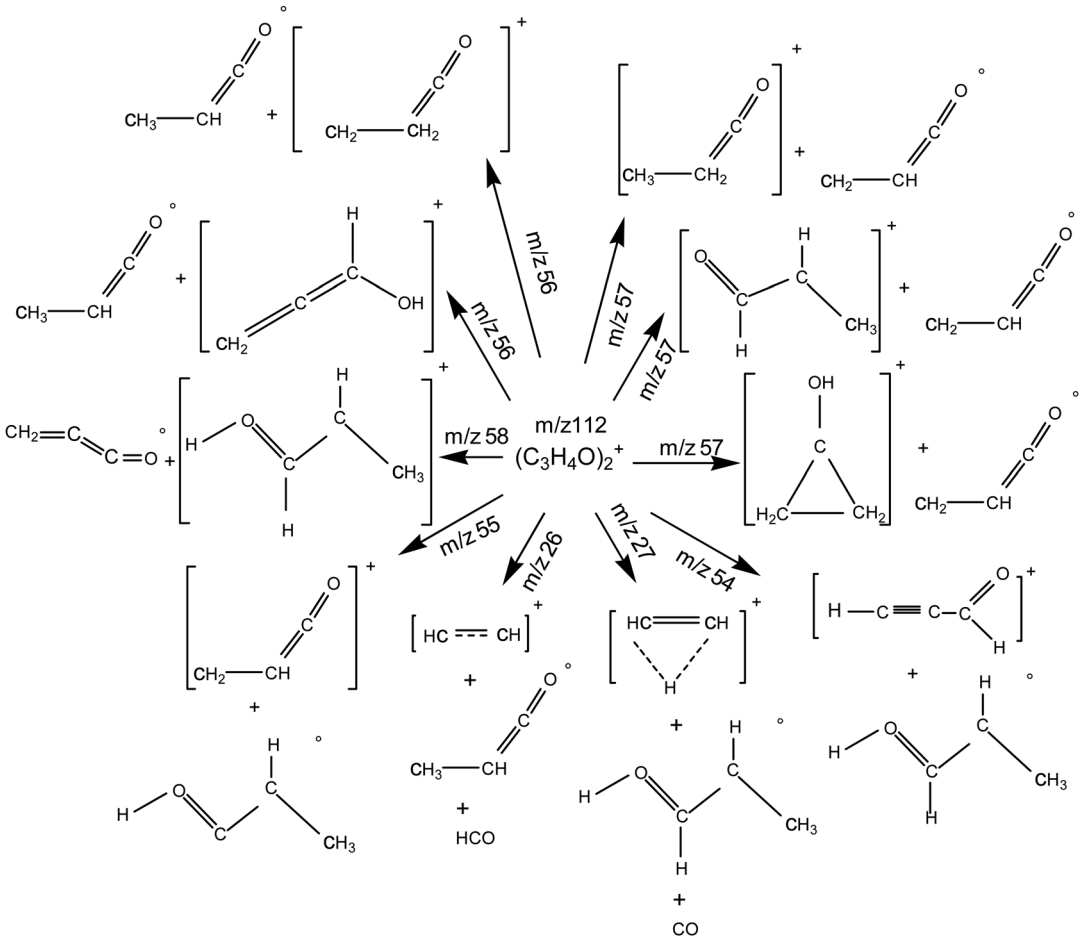

Fig. 9 Fragmentation pathways of the dimer cation MKE_2^+ considered for the quantum-chemical calculations.

bands of the dimer cation. Indeed, upon ionization of neutral van der Waals clusters, the ground state vibrational levels of the ionic cluster are commonly located outside the FC-region accessible *via* direct photoionization of the neutral dimer.[62] The Ar_2^+ dimer has been resolved with the SPES method[68] but a prerequisite is a clear trend in the vibrational envelope which we do not observe in MKE_2 which precludes an experimental determination of the true AIE.

The calculations on the MKE_2 fragmentation show that a few different products can be obtained from dissociative ionization of the dimer. One product, corresponding formally to the addition of two H-atoms to the MKE monomer (*m*/*z* 58) is expected to form around 9.62 eV. Its elemental formula is $C_3H_6O^+$ and the calculated structure is given in Table 5. Another product is *m*/*z* 57 and three different isomers corresponding formally to protonated forms of MKE are expected theoretically at 8.78 eV, 10.11 eV, and 11.47 eV. Also *m*/*z* 55 can be formed from the dissociative photoionization of MKE_2. In the following we discuss the formation of these three ions.

The SPES associated with *m*/*z* 57 and *m*/*z* 58 ions are displayed in Fig. 10. As expected, a slight contribution of the ^{13}C isotopomer signal of the MKE monomer is observed in the *m*/*z* 57 SPES which is presented as a dotted black line in Fig. 10a. With step sizes of 10 meV in the energy scan, we can safely make the assumption that any decipherable isotopic shift due to ^{13}C is minimal and we can use the SPES of the monomer at *m*/*z* 56 to subtract the ^{13}C signal from the total *m*/*z* 57 signal, yielding the filtered signal corresponding to the protonated parent only. This is presented as a solid red line in Fig. 10a. This filtered signal still exhibits some weak signals around and below 9.0 eV which may be an indicator of the formation of the *m*/*z* 57 isomer predicted with AE = 8.78 eV, namely, the propenoyl cation (see Table 5).

In the SPES of the *m*/*z* 57 ion three bands are observed peaking at approximately 9.7, 10.6, and 11.9 eV. The calculations predict cyclopropanol-1-yl to appear at AE = 10.11 eV which agrees with the SPES since this is the onset of the second broad band that extends up to approximately 11.35 eV. Furthermore, the calculations predict the appearance of propanal-2-yl at AE = 11.47 eV, which is also in good agreement with the recorded SPES since this is the origin of the third broad band observed in the SPES. The first broad band, occurring between 9.5 eV and 10.0 eV, can be explained by the following considerations: its onset is unlikely to belong to the propanoyl radical (AE = 8.78 eV), but we note that the first band in the filtered *m*/*z* 57 SPES is quite similarly shaped as the second one that had been assigned to the formation of cyclopropanol-1-yl cation above, only less intense.

Table 5 Calculated and measured AIEs of MKE_2 and the AEs of the different fragmentation pathways of the resulting cation (in eV). The * labels correspond to fragments that were also reported in Table 4 as potential fragments from dissociative ionization of the MKE monomer. However, our computational results shown here indicate that these fragments are more likely formed from dissociative ionization of the MKE_2 dimer. See text for details

	Neutral	Ionization	Fragments											
Formula	$(C_3H_4O)_2$	$(C_3H_4O)_2^+$	$C_3H_6O^+$	$C_3H_3O^+$	$C_3H_5O^+\_1$	$C_3H_5O^+\_2$	$C_3H_4O^+$	$C_3H_4O^+\_1$	$C_3H_3O^+$	$C_3H_2O^+$	C_3H_6O	$C_3H_3^+$	C_3H_4O	$C_2H_2^+$
Molecular structure			C_3H_2O	C_3H_3O	C_3H_3O	C_3H_3O	C_3H_4O	C_3H_4O	C_3H_5O	C_3H_6O	C_3H_6O	+CO	+HCO	
m/z		112	58	57	57	57	56	56	55	54*	27*	26*		
AIE or AE calc.		7.87	9.62	8.78	10.11	11.47	10.20	11.41	10.28	12.18	13.05	13.01		
AIE or AE exptl.		8.75 ± 0.05	9.718 ± 0.05	<9.0	10.10 ± 0.05	11.35 ± 0.05	10.20± 0.05	11.35 ± 0.05	10.30 ± 0.05	12.3 ± 0.1	13.1 ± 0.1	12.9 ± 0.1		

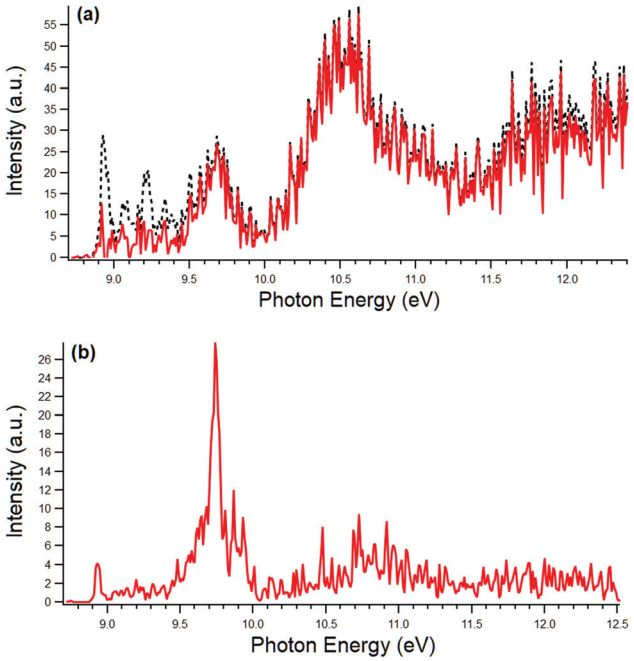

Fig. 10 SPES of the (a) *m/z* 57 and (b) *m/z* 58 fragments formed by dissociative photoionization of the MKE dimer are presented in red. In panel (a), the *m/z* 57 signal which includes both the ^{13}C isotopomer signal of the MKE parent and the protonated MKE parent is displayed with the dotted black line. See text for details.

It is therefore quite likely that first band peaking at 9.7 eV corresponds to the same isomeric cation, only originating from a larger cluster than the dimer. It is quite possible that this band corresponds to the formation of ionized cyclopropanol-1-yl from the dissociative ionization of the trimer, whose signal abruptly cuts off at 9.5 eV (see Fig. S3 in the ESI†). No quantum calculations were carried out for the trimer, so a computational verification of this awaits later work.

Fig. 10b presents the SPES of *m/z* 58. There is a sharp band peaking at 9.72 ± 0.05 eV. With the help of the calculations it can be assigned nicely to the formation of ionized (*E*)-1-propenol, $C_3H_6O^+$ predicted to appear at AE = 9.62 eV from the dissociative photoionization of MKE_2.

From the optimized structure of the neutral dimer and the fragments formed by dissociative ionization we can infer a few potential mechanisms: the optimized geometry of the *m/z* 58 fragment implies a mechanism akin to H_2 addition over the C═O double bond. The structure corresponds to ionized (*E*)-1-propenol and a likely formation mechanism might involve the H2 and H4 atoms in Fig. 8a dissociating from C3 in the upper neutral monomer and form covalent bonds with the O2 and C4 atoms in the monomer below. We suggest this mechanism because the location of the carbonyl group in the upper monomer is too far apart from the closest-located H-atoms in the monomer below, to allow for a facile double H-atom addition.

For the three *m/z* 57 isomers predicted by the calculations we observe two of them definitively in the recorded SPES. The strongest feature in the SPES has been assigned to the formation of the cyclopropanol-1-yl cation. From the optimized geometries

in Fig. 8a, the likeliest formation mechanism would involve a ring-closing between C4 and C6 in the lower monomer while the O2 atom abstracts the H2 atom from the upper monomer. The other *m*/*z* 57 isomer we observe in the SPES, namely propanal-2-yl cation, requires the abstraction of an H-atom by the carbonyl C-atom. This is most likely easily facilitated in the bottom monomer of the neutral where the C4 atom abstracts the H4 atom from the upper monomer.

The ion observed at *m*/*z* 55 that is formed from the monomer MKE^+ by H loss reaction (see above) can also be formed by dissociative photoionization of MKE_2. Contrary to the AE calculation for the MKE + $h\nu \rightarrow$ H + $C_3H_3O^+$ reaction (see Table 3) in the calculations for the MKE_2 + $h\nu \rightarrow$ C_3H_5O + $C_3H_3O^+$ reaction, two isomers for the neutral fragment C_3H_3O have to be considered giving rise to two different AE values, at 9.06 eV and 10.28 eV respectively (see Table 5). As mentioned above and shown in Fig. 4, there was some weak structure observed in the SPES of *m*/*z* 55, with an experimentally observed onset found at AE_a = 10.30 ± 0.05 eV. This threshold could not be explained by dissociative ionization of the MKE monomer. Our calculations, however, provide us with an explanation of this spectral feature since AE_a (*m*/*z* 55) coincides nicely with the formation of the ionized propenoyl radical according to MKE_2 + $h\nu \rightarrow$ C_3H_5O + $C_3H_3O^+$, calculated to appear at AE_{calc} = 10.28 eV.

Finally, the *m*/*z* 54, 27 and 26 experimental appearance energies match the theoretical values for the dissociative ionization and subsequent fragmentation of the MKE dimer rather than the monomer.

3.2.3 Dissociative photoionization of the MKE dimer – *m*/*z* 56. Unimolecular dissociation of the MKE dimer cation is also expected to result in fragments with the same elemental formula as the monomer, *i.e.* $C_3H_4O^+$. Indeed, when the entire *m*/*z* 56 peak from Fig. 1 was treated, some curious broad unresolved signals appeared at energies above the ground state, between 10 and 12.5 eV (labelled AE_A and AE_B, respectively in Fig. 11). Prior PES measurements show that the first excited state of the cation does not appear until 13.3 eV.[16] Our computations at the MRCI/aVTZ level verify this as they find that the first excited state for the MKE^+ ion is located 4.6 eV above neutral MKE ground state (see Table S8, ESI†). This means that other ways had to be found to successfully disentangle the SPES of the MKE parent ion for photon energies in the 9.5–13.3 eV Franck–Condon gap.

The *m*/*z* 56 peak undergoes a significant broadening at higher energies (see Fig. S4, ESI†) and hence we derived a SPES analyzing just the center of the mass peak as well as the total mass peak. The results of this treatment are presented in Fig. 11. We find that the difference between the two treatments left the broad signals (AE_A and AE_B) untouched while the SPES of the monomer ground state was successfully filtered away (*cf.* black line in the upper panel of Fig. 11). The same treatment was applied to the total ion yield (TIY) of the *m*/*z* 56 signal to obtain the TIY curves of MKE individually and the other C_3H_4O fragments (Fig. S5, ESI†).

To assign the broad bands of the difference spectrum we performed additional quantum calculations to account for the dissociation of the dimer back into other isomers of $C_3H_4O^+$. The results of these calculations are presented in Table S5 (ESI†). The calculations predict AEs of two isomers, namely the ionized CH_2CH_2CO biradical, at AE = 10.20 eV, and ionized hydroxypropadiene (CH_2═C═CHOH), at AE = 11.41 eV. The appearance energies calculated for the formation of these two $C_3H_4O^+$ isomers coincide very well with the origin of the broad bands of the difference spectrum presented in Fig. 11, at approximately 10.20 eV and 11.35 eV. Again, the calculations complement the experiment very well to account for the broad signals observed in the *m*/*z* 56 SPES.

4. Astrochemical implications

The simplest molecule to contain a CCO frame, namely ketene, was detected in Sgr B2 with the NRAO 11-m telescope in a dense

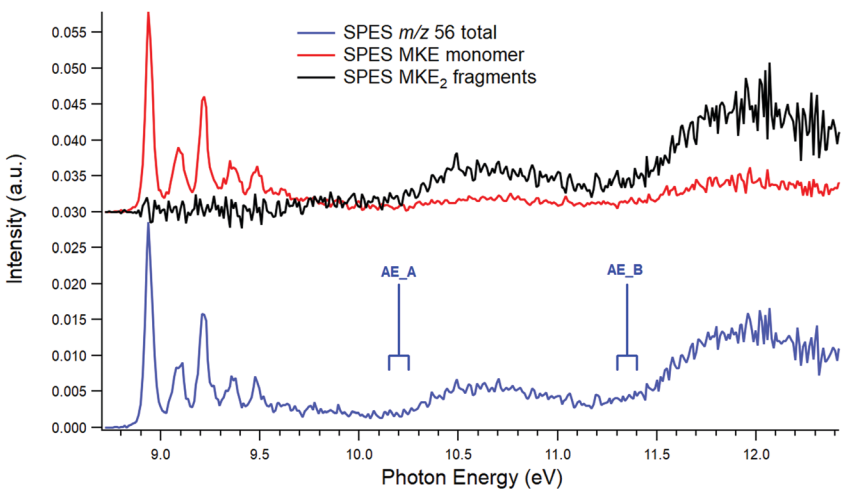

Fig. 11 Lower panel: SPES of the entire *m*/*z* 56 mass peak (*cf.* Fig. 1a; blue line). Upper panel: SPES of the center of the *m*/*z* 56 mass peak (red line). Difference spectrum of both treatments (black line). For further explanations, see text. The pattern observed in the lower pattern could correspond to the formation of isomers of the parent ions from the noncovalent dimer (see Table 5). Two onsets (AE_A and AE_B) are indicated. For further explanations, see text.

region within the Sgr B2 cloud but with relatively low column densities, *i.e.* around 10^{14} cm^{-2}.[15] Ketene is the most stable molecular form of C_2H_2O isomers and the only such isomer to have been detected in the interstellar medium.[69] In terms of such thermochemistry considerations, recent results may provide some insight which is complemented here by our results. Indeed, our results may hold some significant astrochemical implications regarding the potential presence and fate of MKE in the ISM.

As mentioned in the introduction, MKE's isomer propenal has been detected in Sagittarius B2 and TMC-1 along with propanal (C_3H_6O).[70] In the case of propenal, the observations implied a very low temperature (a few K) which precluded an estimate for column densities. Later observations of propenal in the galactic center, however, found abundances around 10^{-9} with respect to H_2.[71]

The most stable form of propenal is 2.8 kJ mol^{-1} more stable than MKE and based on this reasoning, MKE was a viable candidate for detection in space.[19] However, MKE could not be definitely detected in various interstellar regions, but upper limits to its column densities were obtained for dark clouds in different evolutionary stages such as high-mass star-forming regions or cold dark clouds. The largest value of the upper limit of MKE abundance was found in Sgr B2 where values of $(100 \pm 50) \times 10^{14}$ cm^{-2} were inferred. This upper limit is two orders of magnitude larger than the column density of ketene in Sgr B2.

This line of thinking, *i.e.* letting thermodynamic principles guide the search for interstellar molecules has had some successful precedence recently with C_3H_2O structural isomers, however.[72] Thermodynamically, the most stable form of C_3H_2O is found to be propadienone (CH_2CCO – also including the same CCO frame as MKE) but it has continued to elude observations.[73,74] By utilizing quantum chemical calculations it was found that its reaction with a H-atom is barrierless and thus it is now predicted that propadienone undergoes subsequent H-atom additions on grain surfaces to give rise to propenal.[72] whose presence in Sgr B2 is well established.

In comparison with the non-detection of MKE, it is possible that if H-atom addition to MKE is barrierless as well, then this could be a contributing factor for why MKE has eluded detection so far. Thus prior to desorption from the grain mantle, MKE may react without barriers with two H atoms to form a C_3H_6O isomer – either propanal or 1-propenol ($CH_3CHCHOH$). 1-Propenol exists in two different conformers, namely (*E*)- and (*Z*)-1-propenol, neither of which has been detected in space, while the presence of propanal, however, is well documented in Sgr B2.[70] For absolute confirmation, this awaits future work.

Our results, however, give way to another potential scenario for why MKE has eluded detection so far. The ionization energy of MKE is below the Lyman-α limit and hence it is possible that ionization by interstellar VUV radiation depletes the column densities of neutral MKE molecules in these molecular clouds to an extent that they are too small for a definitive detection. We find that the lowest threshold for dissociative ionization is 10.5 eV which gives rise to $C_2H_4^+$ and CO fragments. However, this fragmentation channel does not seem to be very intense and other fragmentation channels (*e.g.* H-loss) could only be reached at higher photon energies. Above 12 eV a wealth of smaller organics can be formed; many of which have already been detected in molecular clouds, but for that reason, their detections cannot be used as any kinds of benchmarks to infer the presence of MKE.

In summary, we present two potentially contributing scenarios for why MKE has not been successfully detected in the ISM. (i) It is hydrogenated prior to desorption and accounting for an increase in the abundance of either propanal or the potential existence of interstellar 1-propenol. Alternatively, (ii) it is ionized by cosmic ray induced photons to such an extent that its (perhaps already small) abundance is further depleted.

Regarding the potential dust-grain formation of MKE, it is widely regarded that formation of COMs in Sgr B2 mostly takes place on dust grains and that two-body gas phase reactions are of limited importance.[70] MKE has already been detected as the product of ice mixtures such as C_3H_6 and CO_2 which have undergone VUV irradiation to induce ice chemistry[20] but definitive formation mechanisms still remain elusive. If solid-state MKE formation is sufficiently efficient on dust grains in Sgr B2 (or other interstellar regions), then one remaining question is whether its desorption mechanism is efficient.

In the laboratory ice study where the formation of MKE was tentatively observed, Hudson *et al.*[20] based their assignments on prior experience with ketene formation in similar ice experiments.[75] Therein, a weak IR feature at 2113 cm^{-1} was observed to stay in the spectra upon heating the ices up to 150 K. With the spectral feature remaining during this warm-up phase might indicate that MKE may not desorb as efficiently from interstellar ices than other organic species in star-forming regions such as Sgr B2.

The question then remains whether the formation yields are high enough that photodesorption of interstellar ice grains containing MKE is sufficient to seed interstellar space with enough MKE for a positive detection. In any case, an active search for the MKE$^+$ cation, which is reasonably stable according to our study, and the (*E*)- and (*Z*)-isomers of 1-propenol, could be a worthwhile future mission to further understand the interstellar chemistry of C_3H_4O isomers.

5. Conclusions

In this work, we studied the single-photon ionization of gas-phase MKE and its dimer by means of VUV synchrotron radiation from 8.7 up to 15.5 eV. In terms of the recorded SPES of MKE, our results here present a significant improvement from previous photoelectron spectra of MKE[16] and can be used for purposes of isomeric disentanglement of the products of interstellar ice analogs.[21] Furthermore, the FC calculated spectrum of MKE reproduced the recorded SPES very well. Measured ionization and dissociative ionization thresholds have been theoretically reproduced using CCSD(T)-F12/cc-pVTZ-F12 calculations in combination with the CV, SR and ZPE corrections, as suggested in the literature. This methodology has been used earlier with some significant success in recent years.[23–25] This allowed the

assignment of experimentally observed masses to the formation of several products of dissociative photoionization of the MKE monomer and dimer. Moreover, we show that photoionization of the van-der Waals dimer MKE_2 gives rise to intramolecular isomerization, H transfer and subsequent unimolecular fragmentation processes, as evidenced by the SPES of fragments corresponding to the addition of one and two H-atoms to the MKE monomer preceding dissociation of dimer. More specifically, the non-covalent character of the dimer is confirmed as its contribution to the formation of MKE fragments could not be explained by solely investigating the dissociative ionization of the monomer. This was demonstrated by theoretical calculations and was key in unravelling the fragmentation patterns observed in our experiment.

In summary, our work showcases the synergy of theoretical and experimental work required to elucidate the photo-induced behavior of MKE and particularly the complications wrought by the dissociative ionization of its dimer. The measured mass spectra, SPES and appearance energies of the products were interpreted with the help of *ab initio* and DFT quantum chemical calculations which highlight the important role theory can play when interpreting experimental data.

Finally, we discuss the potential formation and eventual fates of neutral and ionized MKE in interstellar media and provide suggestions for future molecular targets of observation campaigns to gain a deeper understanding of the chemistry of C_3H_4O isomers in space.

Conflicts of interest

There are no conflicts of interest to declare.

Acknowledgements

This work was supported by the French *Programme National Physique et Chimie du Milieu Interstellaire* (PCMI) of CNRS/INSU with INC/INP co-funded by CEA and CNES. We are grateful to the whole SOLEIL staff for provisions of synchrotron radiation under proposal number 20170203, as well to J.-F. Gil for his technical assistance on the SAPHIRS endstation. We thank Gustavo Garcia for precious help during the measurement campaigns. H.R.H. is grateful for support from the Marie Sklodowska Curie actions, proposal ID: 838372. J.-C. G. thanks the Centre National d'Etudes Spatiales (CNES) for financial support.

References

1 K. I. Öberg, Photochemistry and Astrochemistry: Photochemical Pathways to Interstellar Complex Organic Molecules, *Chem. Rev.*, 2016, **116**(17), 9631–9663, DOI: 10.1021/acs.chemrev.5b00694.

2 H. Linnartz, S. Ioppolo and G. Fedoseev, Atom Addition Reactions in Interstellar Ice Analogues, *Int. Rev. Phys. Chem.*, 2015, **34**(2), 205–237, DOI: 10.1080/0144235X.2015.1046679.

3 E. Herbst and E. F. van Dishoeck, Complex Organic Interstellar Molecules, in *Annual Review of Astronomy and Astrophysics*, ed. R. Blandford, J. Kormendy and E. van Dishoeck, Annual Reviews, Palo Alto, 2009, vol. 47, pp. 427–480.

4 B. A. McGuire, Census of Interstellar, Circumstellar, Extragalactic, Protoplanetary Disk, and Exoplanetary Molecules, *Astrophys. J., Suppl. Ser.*, 2018, **239**(2), 17, DOI: 10.3847/1538-4365/aae5d2.

5 D. M. Paardekooper, J.-B. Bossa and H. Linnartz, Laser Desorption Time-of-Flight Mass Spectrometry of Vacuum UV Photo-Processed Methanol Ice, *Astron. Astrophys.*, 2016, **592**, A67, DOI: 10.1051/0004-6361/201527937.

6 D. M. Paardekooper, J.-B. Bossa, K. Isokoski and H. Linnartz, Laser Desorption Time-of-Flight Mass Spectrometry of Ultraviolet Photo-Processed Ices, *Rev. Sci. Instrum.*, 2014, **85**(10), 104501, DOI: 10.1063/1.4896754.

7 M. Bertin, E. C. Fayolle, C. Romanzin, H. A. M. Poderoso, X. Michaut, L. Philippe, P. Jeseck, K. I. Oeberg, H. Linnartz and J.-H. Fillion, Indirect Ultraviolet Photodesorption from CO:N-2 Binary Ices - An Efficient Grain-Gas Process, *Astrophys. J.*, 2013, **779**(2), 120.

8 K. I. Öberg, R. T. Garrod, E. F. van Dishoeck and H. Linnartz, Formation Rates of Complex Organics in UV Irradiated CH3OH-Rich Ices I. Experiments, *Astron. Astrophys.*, 2009, **504**(3), 891–U28, DOI: 10.1051/0004-6361/200912559.

9 A. Potapov, A. Canosa, E. Jimenez and B. Rowe, Uniform Supersonic Chemical Reactors: 30 Years of Astrochemical History and Future Challenges, *Angew. Chem., Int. Ed.*, 2017, **56**(30), 8618–8640, DOI: 10.1002/anie.201611240.

10 I. R. Cooke and I. R. Sims, Experimental Studies of Gas-Phase Reactivity in Relation to Complex Organic Molecules in Star-Forming Regions, *ACS Earth Space Chem.*, 2019, **3**(7), 1109–1134, DOI: 10.1021/acsearthspacechem.9b00064.

11 B. A. McGuire, A. M. Burkhardt, S. Kalenskii, C. N. Shingledecker, A. J. Remijan, E. Herbst and M. C. McCarthy, Detection of the Aromatic Molecule Benzonitrile (c-C_6H_5CN) in the Interstellar Medium, *Science*, 2018, **359**(6372), 202–205, DOI: 10.1126/science.aao4890.

12 H. Linnartz, J. Cami, M. Cordiner, N. L. J. Cox, P. Ehrenfreund, B. Foing, M. Gatchell and P. Scheier, C_{60}^+ as a Diffuse Interstellar Band Carrier; a Spectroscopic Story in 6 Acts, *J. Mol. Spectrosc.*, 2020, **367**, 111243, DOI: 10.1016/j.jms.2019.111243.

13 K. Taniguchi, Y. Miyamoto, M. Saito, P. Sanhueza, T. Shimoikura, K. Dobashi, F. Nakamura and H. Ozeki, Interferometric Observations of Cyanopolyynes toward the G28.28–0.36 High-Mass Star-Forming Region, *Astrophys. J.*, 2018, **866**(1), 32, DOI: 10.3847/1538-4357/aadd0c.

14 M. A. Cordiner, S. B. Charnley, Z. Kisiel, B. A. McGuire and Y.-J. Kuan, Deep K-Band Observations of TMC-1 with the Green Bank Telescope: Detection of HC_7O, Non-Detection of $HC_{11}N$, and a Search for New Organic Molecules, *Astrophys. J.*, 2017, **850**(2), 187, DOI: 10.3847/1538-4357/aa970c.

15 B. E. Turner, Microwave Detection of Interstellar Ketene, *Astrophys. J.*, 1977, **213**, L75, DOI: 10.1086/182413.

16 H. Bock, T. Hirabayashi and S. Mohmand, Gas-Phase Reactions 21. Thermal Generation of Alkylketenes and Halogenketenes, *Chem. Ber./Recl.*, 1981, **114**(7), 2595–2608, DOI: 10.1002/cber.19811140722.

17 M. Mckee and L. Radom, Structures and Stabilities of $C_3H_4O^+$. Isomers – a G2 Theoretical-Study, *Org. Mass Spectrom.*, 1993, **28**(10), 1238–1244, DOI: 10.1002/oms.1210281040.

18 F. Winther, S. Meyer and F. M. Nicolaisen, The Infrared Spectrum of Methylketene, *J. Mol. Struct.*, 2002, **611**(1–3), 9–22, DOI: 10.1016/S0022-2860(02)00006-6.

19 C. Bermúdez, B. Tercero, R. A. Motiyenko, L. Margulès, J. Cernicharo, Y. Ellinger and J.-C. Guillemin, The Millimeter-Wave Spectrum of Methyl Ketene and the Astronomical Search for It, *Astron. Astrophys.*, 2018, **619**, A92, DOI: 10.1051/0004-6361/201833267.

20 R. L. Hudson, M. J. Loeffler and K. M. Yocum, Laboratory Investigations into the Spectra and Origin of Propylene Oxide: A Chiral Interstellar Molecule, *Astrophys. J.*, 2017, **835**(2), 225, DOI: 10.3847/1538-4357/835/2/225.

21 M. J. Abplanalp, M. Foerstel and R. I. Kaiser, Exploiting Single Photon Vacuum Ultraviolet Photoionization to Unravel the Synthesis of Complex Organic Molecules in Interstellar Ices, *Chem. Phys. Lett.*, 2016, **644**, 79–98, DOI: 10.1016/j.cplett.2015.11.029.

22 F. Goulay, A. J. Trevitt, J. D. Savee, J. Bouwman, D. L. Osborn, C. A. Taatjes, K. R. Wilson and S. R. Leone, Product Detection of the CH Radical Reaction with Acetaldehyde, *J. Phys. Chem. A*, 2012, **116**(24), 6091–6106, DOI: 10.1021/jp2113126.

23 A. Bellili, M. Schwell, Y. Bénilan, N. Fray, M.-C. Gazeau, M. Mogren Al-Mogren, J.-C. Guillemin, L. Poisson and M. Hochlaf, VUV Photoionization and Dissociative Photoionization Spectroscopy of the Interstellar Molecule Aminoacetonitrile: Theory and Experiment, *J. Mol. Spectrosc.*, 2015, **315**, 196–205, DOI: 10.1016/j.jms.2015.05.008.

24 A. Bellili, M. Schwell, Y. Bénilan, N. Fray, M.-C. Gazeau, M. Mogren Al-Mogren, J.-C. Guillemin, L. Poisson and M. Hochlaf, VUV Photoionization and Dissociative Photoionization of the Prebiotic Molecule Acetyl Cyanide: Theory and Experiment, *J. Chem. Phys.*, 2014, **141**(13), 134311, DOI: 10.1063/1.4896987.

25 A. Bellili, Z. Gouid, M. C. Gazeau, Y. Bénilan, N. Fray, J. C. Guillemin, M. Hochlaf and M. Schwell, Single Photon Ionization of Methyl Isocyanide and the Subsequent Unimolecular Decomposition of Its Cation: Experiment and Theory, *Phys. Chem. Chem. Phys.*, 2019, **21**(47), 26017–26026, DOI: 10.1039/C9CP04310A.

26 Z. Chen, K.-C. Lau, G. A. Garcia, L. Nahon, D. K. Božanić, L. Poisson, M. M. Al-Mogren, M. Schwell, J. S. Francisco, A. Bellili and M. Hochlaf, Identifying Cytosine-Specific Isomers via High-Accuracy Single Photon Ionization, *J. Am. Chem. Soc.*, 2016, **138**(51), 16596–16599, DOI: 10.1021/jacs.6b10413.

27 I. Derbali, H. R. Hrodmarsson, Z. Gouid, M. Schwell, M.-C. Gazeau, J.-C. Guillemin, M. Hochlaf, M. E. Alikhani and E.-L. Zins, Photoionization and Dissociative Photoionization of Propynal in the Gas Phase: Theory and Experiment, *Phys. Chem. Chem. Phys.*, 2019, **21**(26), 14053–14062, DOI: 10.1039/c8cp06751a.

28 Z. Gouid, A. Röder, B. K. Cunha de Miranda, M.-A. Gaveau, M. Briant, B. Soep, J.-M. Mestdagh, M. Hochlaf and L. Poisson, Energetics and Ionization Dynamics of Two Diarylketone Molecules: Benzophenone and Fluorenone, *Phys. Chem. Chem. Phys.*, 2019, **21**(26), 14453–14464, DOI: 10.1039/C9CP02385B.

29 Y. Majdi, M. Hochlaf, Y. Pan, K.-C. Lau, L. Poisson, G. A. Garcia, L. Nahon, M. M. Al-Mogren and M. Schwell, Theoretical and Experimental Photoelectron Spectroscopy Characterization of the Ground State of Thymine Cation, *J. Phys. Chem. A*, 2015, **119**(23), 5951–5958, DOI: 10.1021/jp510716c.

30 L. Nahon, N. de Oliveira, G. A. Garcia, J.-F. Gil, B. Pilette, O. Marcouille, B. Lagarde and F. Polack, DESIRS: A State-of-the-Art VUV Beamline Featuring High Resolution and Variable Polarization for Spectroscopy and Dichroism at SOLEIL, *J. Synchrotron Radiat.*, 2012, **19**(4), 508–520, DOI: 10.1107/S0909049512010588.

31 O. Marcouille, P. Brunelle, O. Chubar, F. Marteau, M. Massal, L. Nahon, K. Tavakoli, J. Veteran and J.-M. Filhol, Design, Construction and Magnetic Measurements of the HU640 (OPHELIE2) Undulator Dedicated to the DESIRS VUV Beamline at SOLEIL, in *Synchrotron Radiation Instrumentation Pts 1 & 2*, ed. J. Y. Choi and S. Rah, AIP Conference Proceedings, American Institute of Physics, 2 Huntington Quadrangle, Ste 1No1, Melville, NY 11747-4501 USA, 2007, vol. 879, p. 311.

32 X. Tang, G. A. Garcia, J.-F. Gil and L. Nahon, Vacuum Upgrade and Enhanced Performances of the Double Imaging Electron/Ion Coincidence End-Station at the Vacuum Ultraviolet Beamline DESIRS, *Rev. Sci. Instrum.*, 2015, **86**(12), 123108.

33 G. A. Garcia, B. K. C. de Miranda, M. Tia, S. Daly and L. Nahon, DELICIOUS III: A Multipurpose Double Imaging Particle Coincidence Spectrometer for Gas Phase Vacuum Ultraviolet Photodynamics Studies, *Rev. Sci. Instrum.*, 2013, **84**(5), 053112.

34 G. Garcia, L. Nahon and I. Powis, Two-Dimensional Charged Particle Image Inversion Using a Polar Basis Function Expansion, *Rev. Sci. Instrum.*, 2004, **75**(11), 4989–4996, DOI: 10.1063/1.1807578.

35 J. C. Poully, J. P. Schermann, N. Nieuwjaer, F. Lecomte, G. Gregoire, C. Desfrancois, G. A. Garcia, L. Nahon, D. Nandi, L. Poisson and M. Hochlaf, Photoionization of 2-Pyridone and 2-Hydroxypyridine, *Phys. Chem. Chem. Phys.*, 2010, **12**(14), 3566–3572, DOI: 10.1039/b923630a.

36 H. R. Hrodmarsson, G. A. Garcia, H. Linnartz and L. Nahon, VUV Photoionization Dynamics of the C_{60} Buckminsterfullerene: 2D-Matrix Photoelectron Spectroscopy in an Astrophysical Context, *Phys. Chem. Chem. Phys.*, 2020, **22**, 13880–13892, DOI: 10.1039/D0CP01210F.

37 H. R. Hrodmarsson, G. A. Garcia, L. Nahon, J.-C. Loison and B. Gans, Threshold Photoelectron Spectrum of the Anilino Radical, *J. Phys. Chem. A*, 2019, **123**(42), 9193–9198, DOI: 10.1021/acs.jpca.9b07273.

38 C. Adamo and V. Barone, Toward Reliable Density Functional Methods without Adjustable Parameters: The PBE0 Model, *J. Chem. Phys.*, 1999, **110**(13), 6158–6170, DOI: 10.1063/1.478522.

39 T. Dunning, Gaussian-Basis Sets for Use in Correlated Molecular Calculations 1. the Atoms Boron Through Neon

and Hydrogen, *J. Chem. Phys.*, 1989, **90**(2), 1007–1023, DOI: 10.1063/1.456153.

40 R. Kendall, T. Dunning and R. Harrison, Electron-Affinities of the 1st-Row Atoms Revisited - Systematic Basis-Sets and Wave-Functions, *J. Chem. Phys.*, 1992, **96**(9), 6796–6806, DOI: 10.1063/1.462569.

41 I. M. Mills, Potential Energy Surfaces and Vibrational Anharmonicity, in *Recent Experimental and Computational Advances in Molecular Spectroscopy*, ed. R. Fausto, NATO ASI Series, Springer, Netherlands, Dordrecht, 1993, pp. 79–98, DOI: 10.1007/978-94-011-1974-0_5.

42 M. R. Aliev and J. K. G. Watson, Higher-Order Effects in the Vibration–Rotation Spectra of Semirigid Molecules, in *Molecular Spectroscopy: Modern Research*, ed. K. N. Rao, Academic Press, 1985, ch. 1, pp. 1–67, DOI: 10.1016/B978-0-12-580643-5.50006-3.

43 M. J. Frisch, G. W. Trucks, H. B. Schlegel, G. E. Scuseria, M. A. Robb, J. R. Cheeseman and H. Nakatsuji, *Gaussian 09, Revision E.01*, Gaussian Inc., Wallingford, 2009.

44 M. Lax, The Franck–Condon Principle and Its Application to Crystals, *J. Chem. Phys.*, 1952, **20**(11), 1752–1760, DOI: 10.1063/1.1700283.

45 V. Barone, J. Bloino and M. Biczysko, *Vibrationally-Resolved Electronic Spectra in GAUSSIAN 09*, 2020.

46 J. Bloino, M. Biczysko, F. Santoro and V. Barone, General Approach to Compute Vibrationally Resolved One-Photon Electronic Spectra, *J. Chem. Theory Comput.*, 2010, **6**(4), 1256–1274, DOI: 10.1021/ct9006772.

47 V. Barone, J. Bloino, M. Biczysko and F. Santoro, Fully Integrated Approach to Compute Vibrationally Resolved Optical Spectra: From Small Molecules to Macrosystems, *J. Chem. Theory Comput.*, 2009, **5**(3), 540–554, DOI: 10.1021/ct8004744.

48 J. Bloino, M. Biczysko, O. Crescenzi and V. Barone, Integrated Computational Approach to Vibrationally Resolved Electronic Spectra: Anisole as a Test Case, *J. Chem. Phys.*, 2008, **128**(24), 244105, DOI: 10.1063/1.2943140.

49 J. Bloino, A. Baiardi and M. Biczysko, Aiming at an Accurate Prediction of Vibrational and Electronic Spectra for Medium-to-Large Molecules: An Overview, *Int. J. Quantum Chem.*, 2016, **116**(21), 1543–1574, DOI: 10.1002/qua.25188.

50 T. B. Adler, G. Knizia and H.-J. Werner, A Simple and Efficient CCSD(T)-F12 Approximation, *J. Chem. Phys.*, 2007, **127**(22), 221106, DOI: 10.1063/1.2817618.

51 G. Knizia, T. B. Adler and H.-J. Werner, Simplified CCSD(T)-F12 Methods: Theory and Benchmarks, *J. Chem. Phys.*, 2009, **130**(5), 054104, DOI: 10.1063/1.3054300.

52 T. B. Adler, H.-J. Werner and F. R. Manby, Local Explicitly Correlated Second-Order Perturbation Theory for the Accurate Treatment of Large Molecules, *J. Chem. Phys.*, 2009, **130**(5), 054106, DOI: 10.1063/1.3040174.

53 T. B. Adler and H.-J. Werner, Local Explicitly Correlated Coupled-Cluster Methods: Efficient Removal of the Basis Set Incompleteness and Domain Errors, *J. Chem. Phys.*, 2009, **130**(24), 241101, DOI: 10.1063/1.3160675.

54 A. Koehn and D. P. Tew, Explicitly Correlated Coupled-Cluster Theory Using Cusp Conditions. I. Perturbation Analysis of Coupled-Cluster Singles and Doubles (CCSD-F12), *J. Chem. Phys.*, 2010, **133**(17), 174117, DOI: 10.1063/1.3496372.

55 H.-J. Werner, P. J. Knowles, G. Knizia, F. R. Manby, M. Schütz, P. Celani, W. Györffy, D. Kats, T. Korona, R. Lindh, A. Mitrushenkov, G. Rauhut, K. R. Shamasundar, T. B. Adler, R. D. Amos, S. J. Bennie, A. Bernhardsson, A. Berning, D. L. Cooper, M. J. O. Deegan, A. J. Dobbyn, F. Eckert, E. Goll, C. Hampel, A. Hesselmann, G. Hetzer, T. Hrenar, G. Jansen, C. Köppl, S. J. R. Lee, Y. Liu, A. W. Lloyd, Q. Ma, R. A. Mata, A. J. May, S. J. McNicholas, W. T. F. M. Meyer, III, M. E. Mura, A. Nicklass, D. P. O'Neill, P. Palmieri, D. Peng, K. Pflüger, R. Pitzer, M. Reiher, T. Shiozaki, H. Stoll, A. J. Stone, R. Tarroni, T. Thorsteinsson, M. Wang and M. Welborn, *MOLPRO, Version 2019.2, a Package of Ab Initio Programs*, Cardiff, UK, 2019.

56 K. A. Peterson, T. B. Adler and H.-J. Werner, Systematically Convergent Basis Sets for Explicitly Correlated Wavefunctions: The Atoms H, He, B–Ne, and Al–Ar, *J. Chem. Phys.*, 2008, **128**(8), 084102, DOI: 10.1063/1.2831537.

57 K. A. Peterson and T. H. Dunning, Accurate Correlation Consistent Basis Sets for Molecular Core-Valence Correlation Effects: The Second Row Atoms Al-Ar, and the First Row Atoms B–Ne Revisited, *J. Chem. Phys.*, 2002, **117**(23), 10548–10560, DOI: 10.1063/1.1520138.

58 W. A. de Jong, R. J. Harrison and D. A. Dixon, Parallel Douglas-Kroll Energy and Gradients in NWChem: Estimating Scalar Relativistic Effects Using Douglas-Kroll Contracted Basis Sets, *J. Chem. Phys.*, 2001, **114**(1), 48–53, DOI: 10.1063/1.1329891.

59 J. D. Watts, J. Gauss and R. J. Bartlett, Coupled-cluster Methods with Noniterative Triple Excitations for Restricted Open-shell Hartree–Fock and Other General Single Determinant Reference Functions. Energies and Analytical Gradients, *J. Chem. Phys.*, 1993, **98**(11), 8718–8733, DOI: 10.1063/1.464480.

60 M. Douglas and N. M. Kroll, Quantum Electrodynamical Corrections to the Fine Structure of Helium, *Ann. Phys.*, 1974, **82**(1), 89–155, DOI: 10.1016/0003-4916(74)90333-9.

61 G. Jansen and B. A. Hess, Revision of the Douglas–Kroll Transformation, *Phys. Rev. A: At., Mol., Opt. Phys.*, 1989, **39**(11), 6016–6017, DOI: 10.1103/PhysRevA.39.6016.

62 M. Hochlaf, Advances in Spectroscopy and Dynamics of Small and Medium Sized Molecules and Clusters, *Phys. Chem. Chem. Phys.*, 2017, **19**(32), 21236–21261, DOI: 10.1039/C7CP01980G.

63 H. T. Jonkman, U. Even and J. Kommandeur, Clusters of Organic Molecules in a Supersonic Jet Expansion, *J. Phys. Chem.*, 1985, **89**(20), 4240–4243, DOI: 10.1021/j100266a018.

64 B. Bak, J. J. Christiansen, K. Kunstmann, L. Nygaard and J. Rastrup-Andersen, Microwave Spectrum, Molecular Structure, Barrier to Internal Rotation, and Dipole Moment of Methylketene, *J. Chem. Phys.*, 1966, **45**(3), 883–887, DOI: 10.1063/1.1727700.

65 A. Mahjoub, M. Hochlaf, L. Poisson, N. Nieuwjaer, F. Lecomte, J.-P. Schermann, G. Grégoire, B. Manil, G. A. Garcia and L. Nahon, Slow Photoelectron Spectroscopy of δ-Valerolactam

and Its Dimer, *ChemPhysChem*, 2011, **12**(10), 1822–1832, DOI: 10.1002/cphc.201100090.

66 A. Mahjoub, M. Hochlaf, G. A. Garcia, L. Nahon and L. Poisson, State-Selected Unimolecular Decomposition of δ-Valerolactam^{+} and δ-Valerolactam^{2+} Cations: Theory and Experiment, *J. Phys. Chem. A*, 2012, **116**(34), 8706–8712, DOI: 10.1021/jp3056976.

67 J. Guan, Y. Hu, H. Zou, L. Cao, F. Liu, X. Shan and L. Sheng, Competitive Fragmentation Pathways of Acetic Acid Dimer Explored by Synchrotron VUV Photoionization Mass Spectrometry and Electronic Structure Calculations, *J. Chem. Phys.*, 2012, **137**(12), 124308, DOI: 10.1063/1.4754273.

68 M. Briant, L. Poisson, M. Hochlaf, P. de Pujo, M.-A. Gaveau and B. Soep, Ar 2 Photoelectron Spectroscopy Mediated by Autoionizing States, *Phys. Rev. Lett.*, 2012, **109**(19), 193401, DOI: 10.1103/PhysRevLett.109.193401.

69 E. E. Etim, P. Gorai, A. Das and E. Arunan, Theoretical Investigation of Interstellar C–C–O and C–O–C Bonding Backbone Molecules, *Astrophys. Space Sci.*, 2018, **363**(1), 6, DOI: 10.1007/s10509-017-3226-5.

70 J. M. Hollis, P. R. Jewell, F. J. Lovas, A. Remijan and H. Møllendal, Green Bank Telescope Detection of New Interstellar Aldehydes: Propenal and Propanal, *Astrophys. J.*, 2004, **610**(1), L21–L24, DOI: 10.1086/423200.

71 M. A. Requena-Torres, J. Martin-Pintado, S. Martin and M. R. Morris, The Galactic Center: The Largest Oxygen-bearing Organic Molecule Repository, *Astrophys. J.*, 2008, **672**(1), 352–360, DOI: 10.1086/523627.

72 C. N. Shingledecker, S. Álvarez-Barcia, V. H. Korn and J. Kästner, The Case of H_2C_3O Isomers, Revisited: Solving the Mystery of the Missing Propadienone, *Astrophys. J.*, 2019, **878**(2), 80, DOI: 10.3847/1538-4357/ab1d4a.

73 R. A. Loomis, B. A. McGuire, C. Shingledecker, C. H. Johnson, S. Blair, A. Robertson and A. J. Remijan, Investigating the Minimum Energy Principle in Searches for New Molecular Species—The Case of H_2C_3O Isomers, *Astrophys. J.*, 2015, **799**(1), 34, DOI: 10.1088/0004-637X/799/1/34.

74 J.-C. Loison, M. Agúndez, N. Marcelino, V. Wakelam, K. M. Hickson, J. Cernicharo, M. Gerin, E. Roueff and M. Guélin, The Interstellar Chemistry of H_2C_3O Isomers, *Mon. Not. R. Astron. Soc.*, 2016, **456**(4), 4101–4110, DOI: 10.1093/mnras/stv2866.

75 R. L. Hudson and M. J. Loeffler, Ketene Formation in Interstellar Ices: A Laboratory Study, *Astrophys. J.*, 2013, **773**(2), 109, DOI: 10.1088/0004-637X/773/2/109.

